Journal Name

ARTICLE

Free-standing ultrathin CoMn$_2$O$_4$ nanosheets anchored on reduced graphene oxide for high-performance supercapacitors

Guoxin Gao,[*1] Shiyao Lu[1], Yang Xiang[1], Bitao Dong[1], Wei Yan[2], Shujiang Ding[*1]

Ultrathin CoMn$_2$O$_4$ nanosheets supported on reduced graphene oxide (rGO) are successfully synthesized through a simple co-precipitation method with a post-annealing treatment. With the assistance of citrate, the free-standing CoMn$_2$O$_4$ ultrathin nanosheets can form porous overlays on both sides of rGO sheets. Such a novel hybrid nanostructure can effectively promote the charge transport and accommodate volume variation upon prolonged charge/discharge cycling. When evaluated as a promising electrode for supercapacitors in 6 M KOH solution as electrolyte, the hybrid nanocomposites demonstrate highly enhanced capacitance and excellent cycling stability.

Keywords: Supercapacitor; Nanosheets; CoMn$_2$O$_4$; Graphene

1 Introduction

The fast-growing energy demand for high-power applications, such as electric vehicles and hybrid electric vehicles, has triggered great research efforts in the design and development of novel electrode materials for advanced energy storage devices.[1-3] Supercapacitors, as an important next-generation energy storage/ conversion device, can store a lot of charge temporarily and then release it when needed by a non-faradaic electrical energy storage process, which has attracted intense attention for their high power density, fast charge/discharge process, long cycle life and high reliability.[4-6] They store charge mainly based on either ion adsorption or fast surface redox reactions, which means the performance of the supercapacitors is largely determined by the electrode materials in terms of their morphology, structure, size, porosity and so forth.[7-10] Therefore, the attentions have been strongly paid to fabricating unique electrode materials with large specific surface area for high-performance supercapacitors nowadays.[7, 11, 12]

Nanostructured metal oxides/sulfides/hydroxides, especially owning mesoporous and ultrathin sheet-like structure, have been investigated as advanced electrode materials for supercapacitors widely due to their ultrahigh specific surface area and fast electron/ion-transport pathways.[13-17] Among various metal oxides, ternary cobalt manganate (CoMn$_2$O$_4$) with spinel structure has been considered as a promising electrochemical candidate due to its many advantages such as high theoretical capacity, environmental friendliness, low cost and abundant resources.[18-20] Importantly, Co-Mn oxides-based electrode materials usually demonstrate richer redox reactions over unitary Mn or Co oxides.[21, 22] Obviously, these prominent features are extremely propitious to the application in the high-performance electrochemical energy storage. For examples, Ren *et al.* reported flower-like CoMn$_2$O$_4$ microspheres with mesoporous structure showed a specific capacitance of 188 F g^{-1} at the current density of 1 A g^{-1} in 1 M Na$_2$SO$_4$ solution.[21] Li *et al.* synthesized urchin-like MnCo$_2$O$_4$ hierarchical architectures for supercapacitors in 1 M KOH solution and showed a specific

capacitance of 151.2 F g^{-1} at 5 mV s^{-1}.[23] Additionally, Xu *et al.* fabricated porous CoMn$_2$O$_4$ and MnCo$_2$O$_4$ nanowires via thermal decomposition of organometallic compounds and both of them presented high specific capacitance in 2 M KOH solution.[22] However, the practical application of CoMn$_2$O$_4$-based electrodes is still hindered by the fast capacity fading over extended cycling nowadays, mainly due to the severe agglomeration of the electroactive materials and the heavy destruction of the electrode during the repeated electron/ion insertion and extraction process.[19] Especially cycled at the high current density, the capacity fading becomes far grievous because of the severe aggregation and poor electron/ions conductivity of those electrode materials.[20]

Recently, directly assembling unique nanostructure of the electroactive materials on the conductive substrate (e.g. graphene) becomes an effective strategy to relieve the agglomeration and improve their conductivity and mechanical strength, thus enhancing the cycling stability and the discharge capacitance of the electrodes remarkably.[24-26] For example, Yu *et al.* reported the controllable growth of ultrathin CoMoO$_4$ nanosheets on three dimension graphene as the advanced electrodes for supercapacitors.[27] In addition, Peng *et al.* also fabricated ultrathin NiCo$_2$S$_4$ nanosheets on reduced graphene oxide (rGO) sheets to improve their cyclic stability and specific capacitance greatly.[28] Generally, graphene or rGO in the hybrid nanocomposites could not only increase the electric conductivity, but also provide a flexible support to withstand the huge volume change and drastic structural re-organization of the active materials, thus leading to the enhanced cycling stability.[29, 30]

Herein, we develop a novel hierarchical hybrid nanostructure of reduced graphene oxide supported ultrathin CoMn$_2$O$_4$ nanosheets (rGO@CoMn$_2$O$_4$ NSs) via a simple co-precipitation reaction with a post-annealing treatment. With the assistance of citrate, the CoMn$_2$O$_4$ subunits can be controllably assembled into ultrathin nanosheets, which are free-standing on rGO sheets. When evaluated as the electrodes for supercapacitors in 6 M KOH solution, the resultant rGO@CoMn$_2$O$_4$ NSs manifest high capacitance and excellent cycling stability at the current densities of 4 and 10 A g^{-1}.

2   Experimental Section

2.1 Experimental Details

All the reagents used were supplied by Sigma-Aldrich with analytical grade without further purification. Graphene oxide (GO) was first synthesized based on a modified Hummer's method.[31] In a typical synthesis of rGO supported $CoMn_2O_4$ ultrathin nanosheets, 10 mg of GO was firstly dispersed in 20 mL of absolute ethanol by ultrasonication for about 10 min. Then 20 mL of deionized (DI) water, 0.2 mmol of $Co(NO_3)_2 \cdot 6H_2O$, 0.4 mmol of $Mn(NO_3)_2 \cdot 4H_2O$, 0.5 mmol of hexamethylenetetramine (HMT) and 0.15 mmol of trisodium citrate dihydrate (TSC) were added into the above suspension. After ultrasonication for another 10 min, the suspension was transferred into a round-bottom flask (100 mL) and heated at 90 ^{o}C for 10 h under violently magnetic stirring. After cooling down to room temperature naturally, the black precipitate was harvested by centrifugation and washed with DI water and ethanol for several times. Finally, the obtained product of GO sheets supported Co-Mn nanosheets precursor was dried overnight at 80 ^{o}C and further annealed at 450 ^{o}C for 2 h in N_2 with a heating rate of 1 ^{o}C min^{-1} to obtain well-defined rGO supported $CoMn_2O_4$ ultrathin nanosheets (rGO@$CoMn_2O_4$ NSs). For comparison, the aggregated $CoMn_2O_4$ microspheres were also synthesized under the same condition without adding GO template.

2.2 Characterization

The X-ray diffraction (XRD) patterns were obtained on a Bruker D8 Advanced X-Ray Diffractometer with Ni filtered Cu Kα radiation (λ = 1.5406 Å) at a voltage of 40 kV and a current of 40 mA. Field-emission scanning electron microscope (FESEM) images were carried out on a JEOL JSM-6700F microscope operated at 5 kV. Transmission electron microscope (TEM) images were taken on JEOL JEM-2010 and JEOL JEM-2100F microscopes. Nitrogen sorption measurement was performed on Autosorb 6B at liquid N_2 temperature. Thermogravimetric analysis (TGA) was carried out under air flow of 200 mL min^{-1} with a temperature ramp of 10 ^{o}C min^{-1} to calculate the carbon content in the final nanocomposite. Raman spectroscopy was performed on a Raman spectrometer under a backscattering geometry (λ = 633 nm; Horiba JobinYvon, HR 800).

2.3 Electrochemical measurements

For electrochemical measurement, the working electrodes consist of 70 wt% electroactive materials, 20 wt%carbon black (Super-P-Li) and 10 wt%polymer binder (polyvinylidene fluoride; PVDF). For supercapacitor test, the slurry was pasted onto a piece of nickel foam uniformly and then dried at 120 ^{o}C overnight under vacuum. The electrochemical tests were conducted with a CHI 660D electrochemical workstation in 6.0 M KOH solution as the electrolyte with a three-electrode cell, where Pt foil serves as the counter electrode and a saturated calomel electrode (SCE) as the reference electrode. The specific capacitances were calculated using the following formula:

$$C = \frac{I \bullet \Delta t}{m \bullet \Delta V} \qquad (1)$$

where C, I, m, Δt and ΔV are the specific capacitance (F g^{-1}) of the electroactive materials, the discharging current (A), the mass of the electroactive materials (g), the discharging time (s), and the discharging potential range (V), respectively. The loading of the electroactive materials, namely rGO@$CoMn_2O_4$ NSs, is found to be approximately 1.08 mg cm^{-2}.

3   Results and Discussion

In this present synthesis, two steps are involved to prepare the hierarchical hybrid rGO@$CoMn_2O_4$ NSs, as illustrated in **Figure 1**. Firstly, GO sheets are dispersed into a mixing solution containing Co^{2+}, Mn^{2+}, hexamethylenetetramine (HMT) and trisodium citrate dihydrate (TSC). The metal ions (Co^{2+} and Mn^{2+}) are strongly coordinated with the functional groups (e.g., -COOH, -OH) on GO surface. During the refluxing at 90 ^{o}C, the gradual decomposition of HMT makes the pH value of the solution increasing, which accelerates the formation of Co-Mn precursor on the both sides of GO sheets. Meanwhile, the hydrolysis of TSC produces abundant carboxyl and hydroxyl groups in its molecular structure to further direct the uniform growth of Co-Mn precursor with ultrathin nanosheets standing uprightly on GO surface (GO@Co-Mn precursor). Secondly, the hierarchical precursor is annealed in N_2 at 450 ^{o}C to obtain crystalline $CoMn_2O_4$ NSs with porous morphology following the complete reduction of GO into rGO. As a result, the hierarchical rGO@$CoMn_2O_4$ NSs with a lot of mesopores has been successfully fabricated.
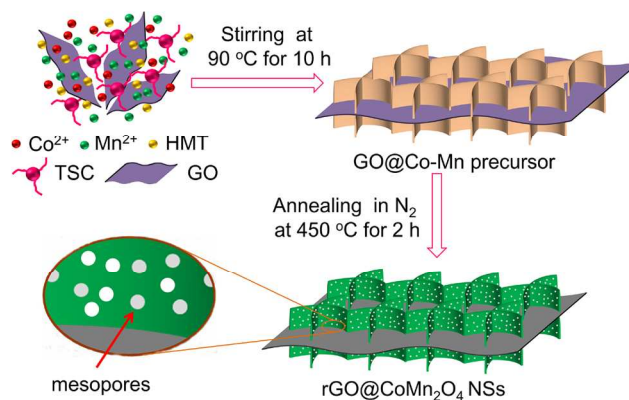

Figure 1. Schematic illustration of the formation process of rGO@$CoMn_2O_4$ NS via a simple co-precipitation reaction and a post annealing treatment.

The crystallographic structure and phase purity of as-prepared ultrathin hierarchical hybrid rGO@$CoMn_2O_4$ NSs are examined by powder X-ray diffraction (XRD) as shown in **Figure 2A**. Obviously, all the identified diffraction peaks are well indexed as the spinel $CoMn_2O_4$ crystalline structure (JCPDS no. 77-0471) after annealed at 450 ^{o}C for 2 h in N_2.[21, 22] No additional diffraction peaks can be detected, implying the absence of any impurities in the hybrid nanocomposite. The morphology and structure of pristine GO sheets, rGO@$CoMn_2O_4$ NSs and aggregated $CoMn_2O_4$ microspheres are further characterized by Field Emission Scanning Electron Microscopy (FESEM). **Figure 2B** reveals that the surface of the pristine GO sheets used is very clean and flat. After the simple co-precipitation reaction, however, large amount of free-standing Co-Mn precursor ultrathin nanosheets is uniformly deposited onto the GO sheets, which can be easily converted to crystalline $CoMn_2O_4$ NSs with well-retained morphology after a post-annealing treatment in N_2 at 450 ^{o}C with a relative slow heating rate of 1 ^{o}C min^{-1} (**Figure 2C**). **Figure 2D** further depicts the close observation of some representative $CoMn_2O_4$ ultrathin nanosheets anchored on the flexible rGO sheets. Apparently, the ultrathin nanosheets are interconnected with each other to form a well-defined hierarchically porous structure standing uprightly on rGO substrate. This novel rGO@$CoMn_2O_4$ NSs hybrid nanostructure is expected to possess good flexibility and strong mechanical strength, which can effectively buffer the volume change of electroactive materials during the repeated charging/discharging process.[32] However, without the support of rGO sheets, only some flower-like $CoMn_2O_4$

microspheres composed of sheet-like subunits are obtained under the same condition (**Figure 2E** and **2F**), suggesting that the GO support is able to prevent the severe aggregation of $CoMn_2O_4$ nanosheets effectively. [33]
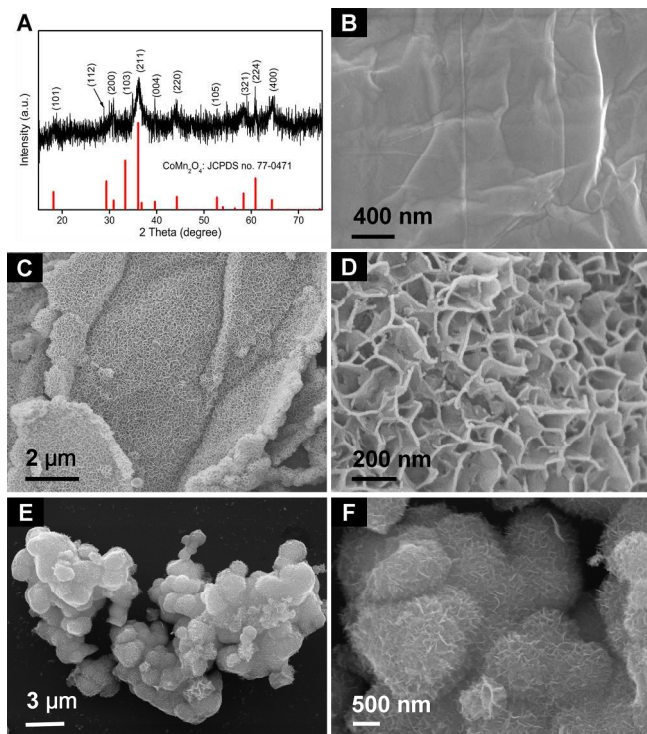

Figure 2. (A) XRD pattern of rGO@$CoMn_2O_4$ NSs. (B-F) FESEM images of (B) GO sheet, (C, D) rGO@$CoMn_2O_4$ NSs obtained with 0.05 mmol of TSC used and (E, F) aggregated $CoMn_2O_4$ microspheres without rGO support.

The intriguing morphology and structure of the resultant rGO@$CoMn_2O_4$ NSs are further elucidated under transmission electron microscopy (TEM). In good agreement with the FESEM results, a low-magnification TEM image (**Figure 3A**) shows that numerous ultrathin $CoMn_2O_4$ NSs are quite loosely standing on the well-retained micro-sized rGO sheets. With a closer observation, the ultrathin nanosheets are around 3 nm in thickness (**Figure 3B**). Remarkably, there are a lot of mesopores within the ultrathin $CoMn_2O_4$ NSs, further disclosing the porous nature of the as-prepared rGO@$CoMn_2O_4$ NSs. The formation of the mesopores within the ultrathin $CoMn_2O_4$ NSs could be related to the gas release during the gradual decomposition of the Co-Mn precursor (hydroxide and carbonate) during the annealing process in N_2.[2] However, due to the low contrast of graphene and the presence of large amount of $CoMn_2O_4$ NSs, the graphene support cannot be directly observed under TEM.[32] Consistent with the XRD analysis, the lattice fringes shown in **Figure 3C** and **3D** can be readily indexed to the (103) and (211) crystal planes of the spinel $CoMn_2O_4$ phase, respectively.[22] Furthermore, the selected area electron diffraction (SAED) pattern (inset of **Figure 3D**) implies a polycrystalline nature of the ultrathin nanosheets.[23]

The porous feature of as-prepared rGO@$CoMn_2O_4$ NSs is further characterized by Brunauer-Emmert-Teller (BET) nitrogen adsorption -desorption measurement. The isothermal plots of N_2 adsorption/desorption for rGO@$CoMn_2O_4$ NSs with a distinct hysteresis loop between adsorption and desorption at the relative pressure of 0.2-0.9 (**Figure S1**, see Supporting Information) demonstrate a typical porous structure.[6] According to the BET equation, the resultant

rGO@$CoMn_2O_4$ NSs show a very high specific surface area of 222.8 m^2 g^{-1}. Additionally, the pore size distributions of the hybrids, calculated from the desorption branch of the isotherm using the Barrett–Joyner–Halenda (BJH) model, are in the range of 1-3 nm. The existence of carbon in the hybrid rGO@$CoMn_2O_4$ NSs can be confirmed through Raman spectroscopy (**Figure S2**, see supporting Information). The characteristic D band and G band are observed at 1353 cm^{-1} and 1590 cm^{-1}, respectively. The D band corresponds to the disordered carbon or defective graphitic structure, while the G band discloses a characteristic feature of graphitic layers, fully confirming the existence of graphene-based carbon in the hybrid nanostructure of rGO@$CoMn_2O_4$ NSs after the annealing treatment. The thermogravimetric analysis (TGA) shows that the content of rGO in the hybrid nanocomposites is about 9.61 wt% (**Figure S3**, see supporting Information). Obviously, such a porous architecture with flexible and conductive graphene support holds great promise in offering sufficient surface area to facilitate electrochemical reactions thus delivering excellent electrochemical performance.[26]
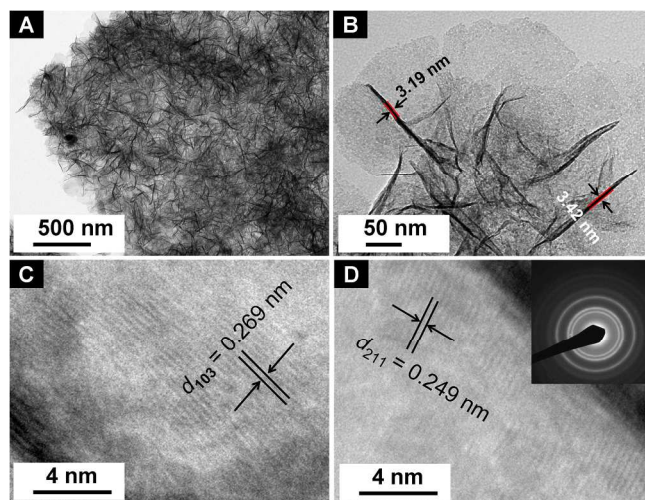

Figure 3. (A, B) TEM and (C, D) HRTEM images of the rGO@$CoMn_2O_4$ NSs obtained with 0.05 mmol of TSC used, inset of D shows their SAED pattern.

In this study, we find that the addition of TSC in the solution is crucial for the successful formation of the ultrathin $CoMn_2O_4$ NSs, which are free-standing on the double sides of rGO sheets. In the absence of TSC, only some irregular $CoMn_2O_4$ nanoparticles or nanospheres can be observed on the surface of rGO substrate due to the coordination effect of the functional groups on rGO sheets (**Figure 4**A). However, when 0.05 mmol of TSC is added into the solution system, the $CoMn_2O_4$ subunits has evolved into ultrathin nanosheets, which are standing uprightly on the surface of rGO (Figure 2C and 2D). The reason should be that the abundant functional groups (such as carboxyl and hydroxyl groups produced by the hydrolysis of citrate) on TSC could facilitate the heterogeneous nucleation and growth of Co-Mn precursor nanosheets on GO support.[32-34] With the amount of TSC increasing to 0.10 mmol (**Figure 4B**), the thickness of the ultrathin $CoMn_2O_4$ NSs increases to about 30 nm probably due to the enhanced coordination effect between the metal ions (Co^{2+} and Mn^{2+}) and the functional groups from TSC, which accelerates the nucleation and growth of Co-Mn precursor nanosheets. Upon further increasing the amount of TSC to 0.15 mmol (**Figure 4C**) and 0.20 mmol (**Figure 4D**), the thickness of the free-standing nanosheets only increases a little, implying that the metal ions have been precipitated completely. Obviously, TSC plays an important role in controlling

the nucleation, growth and thus morphology of the hybrid rGO@CoMn$_2$O$_4$ nanocomposites through the possible coordination effect between metal ions and functional groups of TSC. Thus, the morphology of the resultant rGO@CoMn$_2$O$_4$ hybrid structures can be tuned by simply controlling the amount of TSC in the reaction solution.
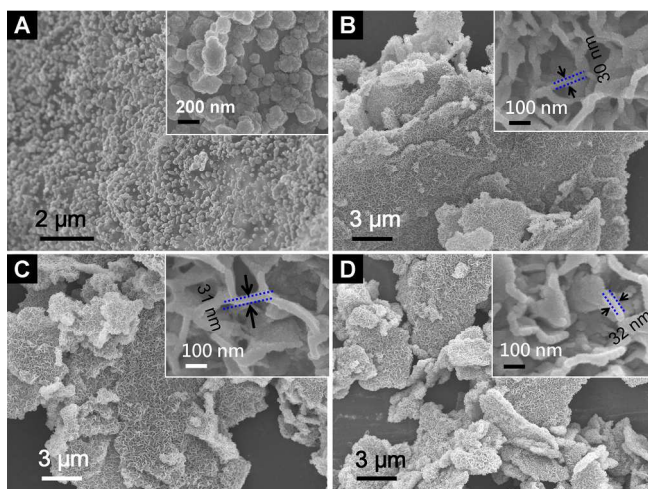

Figure 4. FESEM images of rGO@CoMn$_2$O$_4$ hybrids obtained with various amounts of TSC: (A) 0 mmol, (B) 0.10 mmol, (C) 0.15 mmol, (D) 0.20 mmol.

Subsequently, the electrochemical performance of the resultant rGO@CoMn$_2$O$_4$ NSs was evaluated as the electrode for supercapacitor using 6 M KOH solution as the electrolyte. Figure 5A shows the typical cyclic voltammetry (CV) curves of the rGO@CoMn$_2$O$_4$ NSs electrode with various sweep rates ranging from 5 to 100 mV s^{-1} in the potential window of 0 to 0.5 V *vs.* SCE. Apparently, the shape of the CV curves reveals the pseudocapacitive characteristics.[30] Specifically, a pair of redox peaks can be observed for all sweep rates, which mainly originates from the Faradaic redox reactions related to M-O/M-O-OH (M refers to Co and Mn ions) associated with anions OH$^-$.[26] The redox peaks are located at around 0.33 and 0.43 V when the scan rate is 5 mV s^{-1}. Interestingly, upon increasing the sweep rate from 5 to 100 mV s^{-1}, the redox current increases accordingly. In addition the position of the cathodic peak shifts slightly from 0.33 to 0.31 V. This observation suggests a relatively low resistance of the electrode because of the good contact between the electroactive CoMn$_2$O$_4$ mesoporous nanosheets and the conductive rGO substrate.[2, 11] From the constant current charge/discharge profiles (**Figure 5B**), it can be observed that there are voltage plateaus at about 0.36-0.31 V, which is consistent with the observations in previous reports in the literature. The specific capacitance is calculated by the formula, $C= I\Delta t/(m\Delta V)$. According to the formula, the specific capacitance of the hybrid rGO@CoMn$_2$O$_4$ NSs is evaluated to be ca. 1089.3, 1037.5, 1028.5, 988.1, 958.3, 935.6, 883.3 and 848.9 F g^{-1} at the current densities of 1, 2, 4, 6, 8, 10, 15 and 20 A g^{-1}, respectively, as shown in **Figure 5C**, suggesting the excellent rate capability of the resultant rGO@CoMn$_2$O$_4$ NSs. Those results are remarkable compared to the previously reported values for such CoMn$_2$O$_4$ electrode without growing on conductive substrates.[21, 22] In addition, the cycling stability is also evaluated at the constant current densities of 4 and 10 A g^{-1}, as shown in **Figure 5D**. The specific capacitance is around 1028.4 F g^{-1} in the first cycle and it slightly decreases to 973.8 F g^{-1} even after 5000 cycles at a current density of 4 A g^{-1}. This corresponds to a capacitance loss of only 5.3 %, suggesting an

excellent cycling performance of this hybrid electrode material for supercapacitors. Meanwhile, even cycled at a higher current density of 10 A g^{-1}, the hybrid nanocomposites also can display very good cycling stability. The final specific capacitance as high as 876.1 F g^{-1} can be sustained even after 5000 cycles at such high current density, corresponding to the capacitance loss of about 6.4 %, showing the excellent cyclic stability of the hybrid rGO@CoMn$_2$O$_4$ NSs nanocomposites.
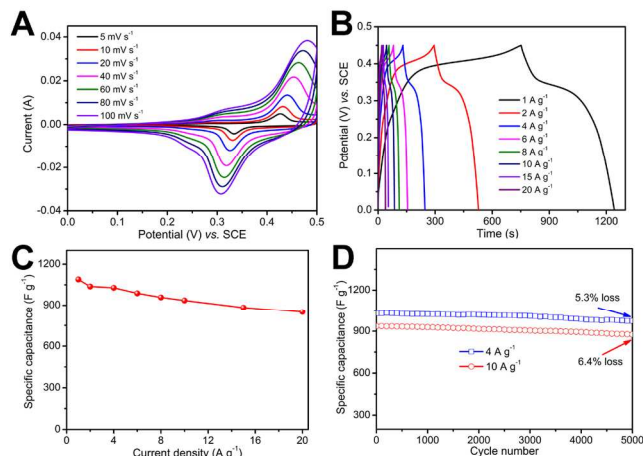

Figure 5. Electrochemical performance of rGO@CoMn$_2$O$_4$ NSs: (A) CV curves at various sweep rates ranging from 5 to 100 mV s^{-1}; (B) Charge-discharge voltage profiles at various current densities ranging from 1 to 20 A g^{-1}; (C) The calculated capacitance as a function of current density according to the data in (B); (D) The capacitance as a function of cycle number at the current density of 4 and 10 A g^{-1}, respectively.

The highly enhanced discharge capacitance and cyclic stability of the free-standing rGO@CoMn$_2$O$_4$ NSs hybrids could be ascribed to the rationally designed nanostructure and composition. Remarkably, the novel hierarchical hybrid nanostructure, in which the ultrathin CoMn$_2$O$_4$ nanosheets are assembled into a hierarchical porous overlay on the flexible and conductive rGO support, will facilitate the electrolyte penetration and electron transport, whilst enhancing the structural integrity of the electroactive materials during the repeated charge/discharge processes.[29, 30] In addition, the porous feature of the ultrathin CoMn$_2$O$_4$ NSs largely increases the amount of the electroactive sites.[11] Just benefiting from these advantageous features, the hierarchical hybrid electrodes manifest high capacitance, and excellent cycling stability.

4 Conclusions

The ultrathin hierarchical CoMn$_2$O$_4$ nanosheets have been grown on flexible and conductive rGO sheets via a simple trisodium citrate (TSC) assisted co-precipitation reaction with a post-annealing treatment. The amount of TSC plays an important role for the assembly of free-standing ultrathin CoMn$_2$O$_4$ nanosheets on rGO sheets. When evaluated as a promising electrode for supercapacitors, these ultrathin nanosheets structures exhibit greatly improved electrochemical performance with very high capacitance and excellent cycling stability. Such hybrid electrodes obtained by directly grown well-defined nanostructures of electroactive materials on flexible rGO sheets might offer great promise for the fabrication of high-performance energy storage device.

Notes and references

1, Department of Applied Chemistry, School of Science, State Key Laboratory for Mechanical Behavior of Materials, Xi'an Jiaotong University, Xi'an 710049, P. R. China.

2, Department of Environmental Science & Engineering, School of Energy & Power Engineering，Xi'an Jiaotong University, Xi'an 710049, P. R. China.

E-mail: guoxingao@mail.xjtu.edu.cn (G. X. Gao);
dingsj@mail.xjtu.edu.cn (S. J. Ding)

1. C. Z. Yuan, B. Gao, L. F. Shen, S. D. Yang, L. Hao, X. J. Lu, F. Zhang, L. J. Zhang and X. G. Zhang, *Nanoscale*, 2011, **3**, 529-545.
2. G. Q. Zhang and X. W. Lou, *Adv. Mater.*, 2013, **25**, 976-979.
3. S. D. Min, C. J. Zhao, Z. M. Zhang, G. R. Chen, X. Z. Qian and Z. P. Guo, *J. Mater. Chem. A*, 2015, **3**, 3641-3650.
4. B. T. Dong, X. Zhang, X. Xu, G. X. Gao, S. J. Ding, J. Li and B. B. Li, *Carbon*, 2014, **80**, 222-228.
5. X. Y. Yu, L. Yu, L. F. Shen, X. H. Song, H. Y. Chen and X. W. Lou, *Adv. Funct. Mater.*, 2014, **24**, 7440-7446.
6. Y. F. Zhang, M. Z. Ma, J. Yang, H. Q. Su, W. Huang and X. C. Dong, *Nanoscale*, 2014, **6**, 4303-4308.
7. Y. F. Zhang, M. Z. Ma, J. Yang, C. C. Sun, H. Q. Su, W. Huang and X. C. Dong, *Nanoscale*, 2014, **6**, 9824-9830.
8. R. J. Zou, Z. Y. Zhang, M. F. Yuen, J. Q. Hu, C. S. Lee and W. J. Zhang, *Sci. Rep.*, 2015, **5**, 10.1038/srep07862.
9. M. C. Liu, L. B. Kong, X. J. Ma, C. Lu, X. M. Li, Y. C. Luo and L. Kang, *New J. Chem.*, 2012, **36**, 1713-1716.
10. L. Q. Mai, F. Yang, Y. L. Zhao, X. Xu, L. Xu and Y. Z. Luo, *Nat. Commun.*, 2011, **2**, 10.1038/ncomms1387.
11. G. X. Gao, L. Yu, H. B. Wu and X. W. Lou, *Small*, 2014, **10**, 1741-1745.
12. D. P. Cai, B. Liu, D. D. Wang, L. L. Wang, Y. Liu, H. Li, Y. R. Wang, Q. H. Li and T. H. Wang, *J. Mater. Chem. A*, 2014, **2**, 4954-4960.
13. C. H. An, Y. J. Wang, Y. A. Huang, Y. A. Xu, C. C. Xu, L. F. Jiao and H. T. Yuan, *Crystengcomm*, 2014, **16**, 385-392.
14. G. Q. Zhang and X. W. Lou, *Sci. Rep.*, 2013, **3**, 10.1038/Srep01470.
15. H. Jiang, J. Ma and C. Z. Li, *Chem. Commun.*, 2012, **48**, 4465-4467.
16. J. P. Liu, J. Jiang, M. Bosman and H. J. Fan, *J. Mater. Chem.*, 2012, **22**, 2419-2426.
17. L. Chen and J. H. Zhu, *Chem. Commun.*, 2014, **50**, 8253-8256.
18. P. Ahuja, V. Sahu, S. K. Ujjain, R. K. Sharma and G. Singh, *Electrochim. Acta*, 2014, **146**, 429-436.
19. S. K. Ujjain, P. Ahuja and R. K. Sharma, *J. Mater. Chem. A*, 2015, **3**, 9925-9931.
20. S. L. Jiang, T. L. Shi, H. Long, Y. M. Sun, W. Zhou and Z. R. Tang, *Nanoscale Res. Lett.*, 2014, **9**, 10.1186/1556-276x-9-492.
21. L. Ren, J. Chen, X. Q. Wang, M. J. Zhi, J. W. Wu and X. H. Zhang, *Rsc Adv.*, 2015, **5**, 30963-30969.
22. Y. Xu, X. Wang, C. An, Y. Wang, L. Jiao and H. Yuan, *J. Mater. Chem. A*, 2014, **2**, 16480-16488.
23. W. Li, K. Xu, G. Song, X. Zhou, R. Zou, J. Yang, Z. Chen and J. Hu, *Crystengcomm*, 2014, **16**, 2335-2339.
24. H. W. Wang, Z. A. Hu, Y. Q. Chang, Y. L. Chen, H. Y. Wu, Z. Y. Zhang and Y. Y. Yang, *J. Mater. Chem.*, 2011, **21**, 10504-10511.
25. L. Huang, D. C. Chen, Y. Ding, S. Feng, Z. L. Wang and M. L. Liu, *Nano Lett.*, 2013, **13**, 3135-3139.
26. L. F. Shen, Q. Che, H. S. Li and X. G. Zhang, *Adv. Funct. Mater.*, 2014, **24**, 2630-2637.
27. X. Z. Yu, B. A. Lu and Z. Xu, *Adv. Mater.*, 2014, **26**, 1044-1051.
28. S. J. Peng, L. L. Li, C. C. Li, H. T. Tan, R. Cai, H. Yu, S. Mhaisalkar, M. Srinivasan, S. Ramakrishna and Q. Y. Yan, *Chem. Commun.*, 2013, **49**, 10178-10180.
29. X. F. Xia, W. Lei, Q. L. Hao, W. J. Wang and X. Wang, *Electrochim. Acta*, 2013, **99**, 253-261.
30. Y. Y. Wei, S. Q. Chen, D. W. Su, B. Sun, J. G. Zhu and G. X. Wang, *J. Mater. Chem. A*, 2014, **2**, 8103-8109.
31. D. C. Marcano, D. V. Kosynkin, J. M. Berlin, A. Sinitskii, Z. Z. Sun, A. Slesarev, L. B. Alemany, W. Lu and J. M. Tour, *Acs Nano*, 2010, **4**, 4806-4814.
32. G. Gao, H. B. Wu, B. Dong, S. Ding and X. W. Lou, *Adv. Sci.*, 2015, **2**, 1400014.
33. G. Gao, H. B. Wu and X. W. Lou, *Adv. Energy Mater.*, 2014, **4**, 201400422.
34. L. Ge, X. Y. Jing, J. Wang, J. Wang, S. Jamil, Q. Liu, F. C. Liu and M. L. Zhang, *J. Mater. Chem.*, 2011, **21**, 10750-10754.

Graphical Abstract
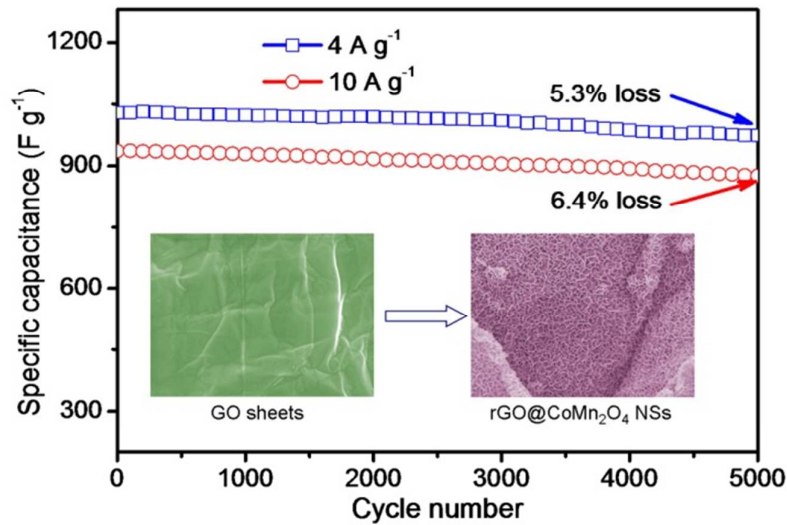
Free-standing ultrathin $CoMn_2O_4$ nanosheets are successfully assembled on reduced graphene oxide via a simple trisodium citrate (TSC) assisted co-precipitation method with a post-annealing treatment. When evaluated as the electrodes for supercapacitors in 6 M KOH solution, the as-prepared rGO@CoMn₂O₄ NSs manifest high capacitance and excellent cycling stability at the current densities of 4 and 10 A g⁻¹.